Modeling and control of a transfemoral prosthesis embedding two infinitely variable transmissions

Renaud Ronsse, Matthias Tummers, Christophe Everarts

Modeling and Control of a Transfemoral Prosthesis Embedding two Infinitely Variable Transmissions*

Renaud Ronsse[1,2], Matthias Tummers[1], and Christophe Everarts[1]

***Abstract*— In this paper, we report the model of an original actuation concept for a transfemoral prosthesis, relying on the combination of a single power motor, a compliant element (a spring), a mechanical differential, and two infinitely variable transmissions. It allows to manage the mechanical power flows through the device in both directions (i.e. when energy should be produced or dissipated by the knee and ankle), so that the power motor does not face the sharp load power fluctuations. The paper further reports a preliminary approach to synthesize a closed-loop controller for this device, and simulation results of this closed-loop behavior for three locomotion tasks: level-ground walking and stair ascent/descent. These results illustrate the capacity of this actuation principle to filter the load power profile, and further highlight the necessity to maximize the mechanical efficiency of each part of this actuation scheme.**

I. INTRODUCTION

Ideally, active leg prostheses should be able to produce the same locomotion profiles as a sound leg. This is however a critical challenge for the prosthesis designer, because the kinematic and torque profiles of the leg joints are highly fluctuating within a gait cycle and across locomotion tasks. Fig. 1 shows the knee and ankle profiles for level ground walking and stair ascent/descent (data taken from [1], [2]). It illustrates the above statement: over the cycle, both the velocity and torque profiles oscillate between large extremes and cross the zero line several times. So does the power profile, since it is the product of both. The prosthesis actuators and mechanical parts should thus be dimensioned in order to potentially fulfill similar specs.

Integrating the power profiles over time reveals the energy balance of the joint during the corresponding task: if this energy is positive, the corresponding joint produces energy during the cycle, e.g. to propel the body forward; if negative, the joint dissipates energy during the cycle, e.g. to dissipate potential energy during stair descending (Table I). Intuitively, during stair ascending (resp., descending), both joints produce (resp., dissipate) energy, mainly in order to vary the level of potential energy of the body. Interestingly, the level-ground walking cycle is unbalanced: while the ankle produces energy – mainly in late stance in order to propel the body forward –, the knee dissipates. Furthermore, data reveal

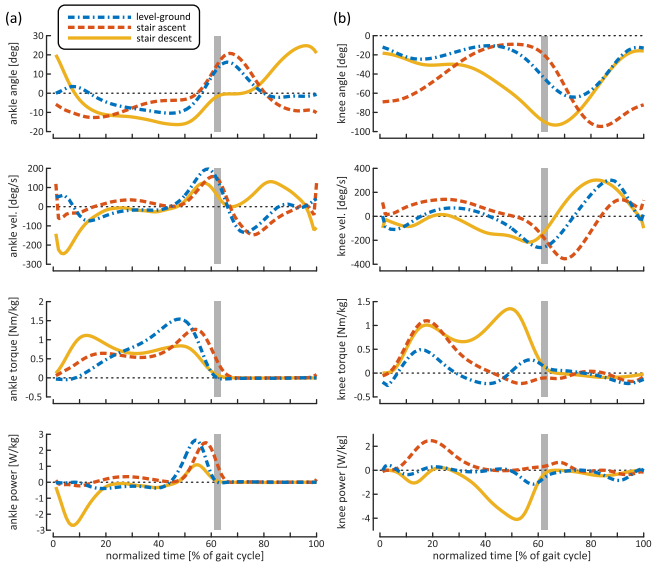

Fig. 1. From top to bottom: ankle (a) and knee (b) angular position and velocity, torque, and power profiles, as function of the normalized gait cycle phase (in %) and for the three different tasks. 0% and 100% capture two successive foot strikes, while the shaded gray rectangles capture the transition from stance to swing. The torque and power profiles are normalized by the subject's weight (in kg). Positive/negative values capture plantarflexion/dorsiflexion for the ankle (a), and extension/flexion, for the knee (b), respectively. Data taken from [1], [2].

that the knee dissipates more than what the ankle produces, so that – in theory – globally passive transfemoral prostheses could reproduce the healthy knee and ankle profiles [3], [4].

Nowadays transfemoral amputees do not use integrated prostheses, but rather combine appropriate knee and ankle modules. The simplest and cheapest ankle prostheses are passive, i.e. have no embedded actuators. They are capable of storing energy in elastic elements and returning a majority

TABLE I

AVERAGE CYCLE PERIOD AND ENERGY BEING PRODUCED (IF POSITIVE) OR DISSIPATED (IF NEGATIVE) BY THE THE ANKLE AND KNEE JOINTS, FOR THE THREE CONSIDERED TASKS. THIS ENERGY IS NORMALIZED BY THE SUBJECT'S WEIGHT (IN KG). DATA ADAPTED FROM [1], [2].

	Level-ground walking	Stair ascending	Stair descending
Period [s]	1.17	1.45	1.26
Ankle energy [J/kg]	0.164	0.404	−0.325
Knee energy [J/kg]	−0.223	0.671	−1.146

*This work was supported by the EU within the CYBERLEGs (FP7-ICT-2011-7 Grant Agreement #287894) and CYBERLEGs++ projects (H2020-ICT-2016-1 Grant Agreement #731931).

[1]The authors are with the Center for Research in Mechatronics, the Institute of Mechanics, Materials, and Civil Engineering, and the "Louvain Bionics" consortium, Université catholique de Louvain, 1348 Louvain-la-Neuve, Belgium renaud.ronsse@uclouvain.be

[2]Renaud Ronsse is further with the Institute of Neuroscience, Université catholique de Louvain, 1200 Brussels, Belgium

of this energy to assist in forward propulsion [5]. More advanced elastic prostheses also embed an actuated clutch, to release the elastic energy at the most appropriate time [6]. The main drawback of these passive solutions is that they cannot reproduce the positive mechanical work of a normal ankle, even during level-ground walking [7], since they can only provide the energy that was stored during the earlier phase. This gap is bridged by the next generation of ankle prostheses, being equipped with power actuator [8]. Interestingly, these prototypes often rely on the concept of Series Elastic Actuator [9], since they embed a compliant element between their actuator and the ankle joint. This allows storing-and-releasing energy during the walking phases, such that the motor undergoes smaller displacements and thus faces smaller power peaks. Such a device recently proved to normalize the gait pattern of trans-tibial amputees, both regarding kinematics and metabolic cost [10], [11].

In contrast to the ankle, a power actuator is not necessary in a knee module to reproduce natural kinematics and dynamics, at least for level-ground walking. The simplest knee prostheses are hinge joints being locked during walking and unlocked only for sitting, thus producing unaesthetical gaits. More recent evolutions rely on servo-controlled springs and dampers. However, none of these solutions are capable of emulating a sound knee behavior during stair climbing, since they do not produce energy.

A limited amount of research prototypes addressed an integrated design for the knee and ankle replacement. Integration offers more flexibility to optimize the mechanical design and to share resources like battery or electronics, see e.g. [12]. Others exploited the unbalance in energy production and dissipation of the knee and ankle joints through entirely passive transfemoral prostheses with mechanical energy transfer [3], [4]. Recently, such an energy transfer mechanism was further combined with an active integrated prosthesis [13].

In this paper, we also aim at achieving energy transfers between both joints, although we adopt a radically different framework. Moreover, our approach targets not only level-ground walking, but also stair ascent or descent, i.e. tasks with a net positive or negative energy balance [2], [12]. Our approach also relies on a compliant element storing energy, but is so that this energy can be flexibly released or harvested by using Infinitely Variable Transmissions (IVTs). IVTs are special sort of Continuously Variable Transmissions (CVTs), so that they can produce both positive and negative transmission ratios. CVTs and IVTs were initially designed for the automobile industry in order to enable the car engine to run at its most efficient rotational velocity for a large range of vehicle speeds. Recently, it was extended to robotic applications requiring compliance and energy efficiency (the V2E2 concept of [14]). We [15] and others [16] studied this principle for single joint lower-limb prostheses. In particular, we figured out that such a prosthesis requires to change the IVT transmission ratio at low-to-zero rotational velocity, a feature which is not achieved by existing IVTs. Consequently, we developed our own IVT concept having the capacity to change the transmission ratio whatever the rotational velocity [17].

In sum, an active transfemoral prosthesis which can reproduce healthy patterns in different locomotion tasks should follow highly varying kinematic and dynamic profiles, while producing or dissipating mechanical energy with one or both of its joints. The goal of this paper is to provide a new actuation concept for such a prosthesis, and to report the benefits it could bring regarding efficiency and reduction of the power peaks. Section II builds up the model of this new actuation concept. Section III reports a preliminary design of a closed-loop controller of such a prosthesis, in order to achieve proper torque tracking at both the knee and ankle. Section IV reports simulated results of this feedback controlled prosthesis, for the three tasks mentionned above. The paper ends with a conclusion.

II. MODEL OF A TRANSFEMORAL PROSTHESIS WITH TWO IVTS

This section overviews the conceptualization of an active transfemoral prosthesis achieving flexible power flows management, by embedding two IVTs. Extending the approach of [14], [18], we developed an integrated actuator for such a prosthesis by appropriately combining a power actuator, a compliant element storing mechanical energy, and *two* IVTs which modulate the output torques as a function of the available energy. More precisely, we extended the V2E2 concept of [14], as pictured in Fig. 2.

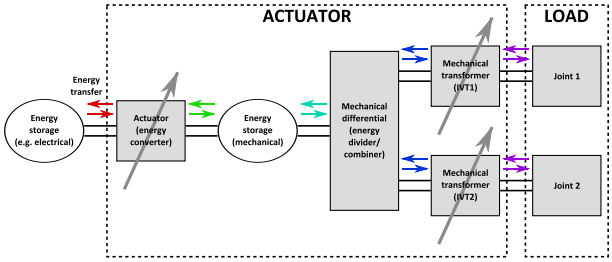

Fig. 2. Actuator concept for a load having two degrees of freedom, i.e. two joints. The gray arrows capture the fact that the amount of energy being converted or transferred can be varied. The color code of the power flows is consistent with the profiles of Figs. 4a and 5.

The V2E2 concept is a single joint actuator, having thus no mechanical differential as in Fig. 2. In this concept, the IVT is used to modulate its output torque $\tau_{\iota,out}$, i.e. the torque actuating the load joint, across positive and negative values, and whatever its input torque $\tau_{\iota,in}$ (pending it is $\neq 0$). Indeed, the input and output torques of an IVT are – by definition – related to each other through the instantaneous transmission ratio $\rho_\iota(t)$, i.e.:

$$\tau_{\iota,out}(t) = \rho_\iota(t)\tau_{\iota,in}(t). \quad (1)$$

Note that (1) assumes a perfect IVT, i.e. with efficiency equal to 1. This assumption will be relaxed later on.

The V2E2 concept reveals its main interest when considering that a compliant element – providing mechanical energy storage – is used as an intermediate step in order to produce $\tau_{\iota,in}$. Assuming this compliant element is a spring,

it produces a torque τ_s equal to the product of its stiffness k and deformation θ_s, i.e.:

$$\tau_s(t) = k\theta_s(t). \tag{2}$$

Combining (1) and (2) (with $\tau_{\iota,in} = \tau_s$) reveals that the V2E2 can provide *any* desired positive or negative torque $\tau_{\iota,out}(t)$, whatever $\theta_s(t)$ (pending it is $\neq 0$), by properly controlling the transmission ratio, i.e.:

$$\rho_\iota(t) = \frac{\tau_{\iota,out}(t)}{k\theta_s(t)}. \tag{3}$$

Consequently, if negative work is done on the load, i.e. if the load produces energy that needs to be "dissipated" by the actuator, this work would not be lost but instead stored in the compliant element. In sum, this actuator could exactly render any physical impedance by storing or releasing energy in/from the spring. A consequence of this statement – critical for applications with varying power profiles – is that the compliant element can be used as a buffer of mechanical energy, so that the power actuator providing (and dissipating) mechanical energy to/from the spring faces a much smoother power profile than the one of the load [15].

In the present paper, we extend this concept for actuating two degrees of freedom, i.e. the knee and ankle joints of a lower-limb prosthesis. This is achieved by augmenting the V2E2 concept as pictured in Fig. 2, i.e. with a mechanical differential distributing the mechanical power flow through both joints. Interestingly, this architecture offers not only to store negative work produced by the load and to smooth the power profile, but also to achieve this *across* both joints. Said differently: (i) if one joint produces energy while the other dissipates (like in level-ground walking), the power flows through the differential naturally adapt; and (ii) the main actuator faces a power profile being a smoothed version of the *sum* of both joints' profiles. These statements will be detailed in the following sections, providing a model of the successive elements of Fig. 2. These models follow the concept of power ports like in [14]. They consist in every domain of a coupled pair of variables called effort and flow. In the electric domain, these are the voltage (effort) and current (flow); in the mechanical domain, these are the force or torque (effort) and (rotational) velocity (flow). Importantly, the product of the effort and the corresponding flow is equal to the power being instantaneously transferred through that port, whatever the domain. Flows are considered to be positive if entering into the corresponding port, both from the "input" and "output" sides. This explains the sign convention adopted in Eqs. (4), (7), (10), (11), and Table II.

A. Model of the loads

Ideally, the loads should be modeled as admittance operators: each load joint rotates with a velocity ω_l depending on the torque it receives from the IVT $\tau_l = \tau_{\iota,out}$, internal state variables and dynamical parameters. However, when the load joints are the knee and ankle of an active prosthesis, these operators should account not only for the prosthesis dynamics, but also for the dynamics of the rest of the body and – more critically – for the adaptive motor control strategy of the amputee walking with the prosthesis. In order to avoid this huge modeling effort, in the present work, we assume the load joints to always follow the kinematic profiles from Fig. 1, whatever the torque they receive. We assume that this provides a good approximation of the whole device dynamic behavior when the steady-state torques and kinematic profiles are close to those of Fig. 1. Note finally that the loads are not necessarily passive: Table I revealed that – in some cases – the leg joints produce energy through the gait cycle.

B. Model of the IVTs

An IVT is a mechanical transmission whose output velocity $\omega_{\iota,out}$ equals the input one $\omega_{\iota,in}$, divided by the time-varying transmission ratio ρ_ι:

$$\omega_{\iota,out}(t) = -\omega_{\iota,in}(t)/\rho_\iota(t). \tag{4}$$

Ideally, power is conserved through an IVT, so that the input/output torques obey the opposite relationship (see (1)). However, in the real world, no mechanical transmission displays a perfect efficiency. This fact must be accounted for in a contribution like the present one, where the global energetic performance of the device is a central point. Therefore, (1) is replaced by:

$$\tau_{\iota,out}(t) = \eta_\iota(t)\rho_\iota(t)\tau_{\iota,in}(t) \tag{5}$$

where $\eta_\iota(t)$ is the (time-varying) IVT efficiency. For the sake of simplicity, we will neglect situations where the IVT gears are stuck (see e.g. [19] for more details). Consequently, the IVT efficiency will be captured by a coefficient smaller than one if the IVT brings power to the joint and the inverse of this coefficient otherwise. In mathematical terms:

$$\eta_\iota(t) = \begin{cases} \tilde{\eta}_\iota & \text{if } \tau_{\iota,in}(t)\omega_{\iota,in}(t) > 0 \\ 1 & \text{if } \tau_{\iota,in}(t)\omega_{\iota,in}(t) = 0 \\ 1/\tilde{\eta}_\iota & \text{if } \tau_{\iota,in}(t)\omega_{\iota,in}(t) < 0 \end{cases} \tag{6}$$

where $0 \leq \tilde{\eta}_\iota < 1$.

C. Model of the differential

A mechanical differential has three mechanical shafts, thus its model has three ports. Since it is a passive device which cannot store energy, at every moment, at least one of them must face a positive power while at least another faces negative power. Following the layout of Fig. 2, the port on the spring side is called the "input", and the ports on the IVTs side the "outputs". The velocity relationship is thus:

$$\chi_d\omega_{d,out1}(t) + (1-\chi_d)\omega_{d,out2}(t) = -\omega_{d,in}(t) \tag{7}$$

where $\omega_{d,in}$, $\omega_{d,out1}$, and $\omega_{d,out2}$ denote the input and outputs velocities, respectively, and $0 < \chi_d < 1$ is a constant parameter capturing possibly different transmission ratios between the input and both outputs. Similarly, the torque relationships are:

$$\tau_{d,out1}(t) = \eta_{d1}(t)\chi_d\tau_{d,in}(t), \tag{8}$$

$$\tau_{d,out2}(t) = \eta_{d2}(t)(1-\chi_d)\tau_{d,in}(t). \tag{9}$$

Similarly to η_t in (5), η_{d1} and η_{d2} capture the time-varying efficiencies of the differential, varying as a function of the direction of the power flows:

$$\eta_{d1}(t) = \begin{cases} \tilde{\eta_d} & \text{if } \tau_{d,in}(t)\omega_{d,in}(t) > 0 \text{ and } \tau_{d,out1}(t)\omega_{d,out1}(t) \leq 0 \\ 1 & \text{if } \tau_{d,in}(t)\omega_{d,in}(t) > 0 \text{ and } \tau_{d,out1}(t)\omega_{d,out1}(t) > 0 \\ 1 & \text{if } \tau_{d,in}(t)\omega_{d,in}(t) \leq 0 \text{ and } \tau_{d,out1}(t)\omega_{d,out1}(t) \leq 0 \\ 1/\tilde{\eta_d} & \text{if } \tau_{d,in}(t)\omega_{d,in}(t) \leq 0 \text{ and } \tau_{d,out1}(t)\omega_{d,out1}(t) > 0 \end{cases} \quad (10)$$

where $0 \leq \tilde{\eta_d} < 1$ is the coefficient governing efficiency as a function of the power flows direction. A similar equation exists for $\eta_{d2}(t)$.

D. Model of the compliant element (spring)

The compliant element is a spring whose torque-to-deformation relationship has been given in (2). Importantly, a spring is a dynamical element. It is thus governed by a state equation capturing the rate of change of its deformation as a function of its input and output velocities:

$$\dot{\theta}_s(t) = \omega_{s,out}(t) + \omega_{s,in}(t). \quad (11)$$

E. Model of the power actuator

The actuator in Fig. 2 is in charge of the conversion between the mechanical energy being dissipated or produced by the joints, and another type of energy being stored. We assume this actuator to be a DC motor, so that this external energy is electrical, stored e.g. in a battery. Equations capturing the dynamics of such a motor are typically:

$$u_m(t) = K_m\omega_{m'}(t) + R_m i_m(t); \quad (12)$$

$$J_{m'}\dot{\omega}_{m'}(t) = K_m i_m(t) - \tau_f(t) - \tau_{m'}(t). \quad (13)$$

In (12), u_m denotes the input voltage (effort) and i_m the motor current (flow); R_m and K_m are the motor parameters, i.e. the armature resistance and back electromotive constant; and $\omega_{m'}$ is the state variable, i.e. the motor shaft velocity. Note that this so-called electrical equation neglects the armature inductance, which is a frequent assumption [20]. Eq. (13) captures the relationship between the motor current and produced torque $\tau_{m'}(t)$, $J_{m'}$ being the motor inertia, and $\tau_f(t)$ capturing all friction torques in the motor. Such a motor would often be connected to a gearbox of ratio χ_g, whose output velocity and torque are thus given by:

$$\omega_m(t) = \omega_{m'}(t)/\chi_g, \quad (14)$$

$$\tau_m(t) = \eta_g(t)\left(\chi_g\tau_{m'}(t) + J_g\dot{\omega}_m(t)\right). \quad (15)$$

TABLE II

EFFORT AND FLOW RELATIONSHIPS BETWEEN THE BLOCKS IN FIG. 2.

	Effort	Flow
Actuator to spring	$\tau_m = k\theta_s$	$\omega_{s,in} = \omega_m$
Spring to differential	$\tau_{d,in} = k\theta_s$	$\omega_{d,in} = -\omega_{s,out}$
Differential to IVTs	$\tau_{t1,in} = \tau_{d,out1}$ and $\tau_{t2,in} = \tau_{d,out2}$	$\omega_{t1,in} = -\omega_{d,out1}$ and $\omega_{t2,in} = -\omega_{d,out2}$
IVTs to loads	$\tau_{l1} = \tau_{t1,out}$ and $\tau_{l2} = \tau_{t2,out}$	$\omega_{l1} = -\omega_{t1,out}$ and $\omega_{l2} = -\omega_{t2,out}$

where $\eta_g(t)$ captures the gearbox efficiency and obey a similar equation as (6), and J_g captures the gearbox inertia. Rearranging (12-15) gives the motor+gearbox state equation:

$$J_m\dot{\omega}_m(t) = \frac{-K_m^2}{R_m}\omega_m(t) + \frac{K_m}{\chi_g R_m}u_m(t) - \frac{1}{\chi_g}\tau_f(t) - \frac{1}{\eta_g(t)\chi_g^2}\tau_m(t), \quad (16)$$

where $J_m = J_{m'} + J_g/\chi_g^2$ is the equivalent motor+gearbox inertia. By convention, we consider ω_m to be positive when going out of the motor port. It is thus equal to the opposite of the motor's output flow.

F. Block connections

The various blocks modeled in the sections above are actually connected to each other, according to Fig. 2. Therefore, trivial relationships exist between the effort and flow variables of the different blocks, as summarized in Table II. In this table, variables associated to the first and second loads and IVTs are denoted with a subscript 1 and 2, respectively.

G. Model of the IVT actuation units

Last but not least, this section provides a model of the IVT actuators, i.e. the mechanisms actually varying the transmission ratios ρ_{t1} and ρ_{t2}. This model relies on the IVT design reported in [17]. In short, the transmission ratio of this IVT is changed by controlling the position x_t of an external ring, rolling on the tilted conical planets of a modified planetary gear. The relationship between x_t and the actual transmission ratio is (see [17] for details):

$$\rho_t(t) = 1 - \frac{R}{\sin\alpha\, x_t(t)}, \quad (17)$$

where R is a gain depending on the size of the various IVT gears, and α is the inclination angle of the tilted planets. Controlling x_t is achieved through a lead screw and a similar DC motor as the one described in Section II-E:

$$J_{mt}\xi\ddot{x}_t(t) = \frac{-K_{mt}^2}{R_{mt}}\xi\dot{x}_t(t) + \frac{K_{mt}}{R_{mt}}u_{mt}(t), \quad (18)$$

where ξ is the lead screw pitch, and J_{mt} the equivalent inertia of the motor, lead screw and IVT ring. We assume that this mechanism faces no friction.

III. CLOSED-LOOP CONTROL

The model outlined in Section II is a redundant system: it has 3 inputs, represented by the arrows in Fig. 2 (the voltage of the main power actuator u_m and the voltages of the IVT actuators u_{mt1} and u_{mt2}), but only 2 reference signals to track, namely the reference torques to be transmitted to the joints ($\tau_{ref,l1}$ and $\tau_{ref,l2}$). In this section, we report synthesis methods for designing closed-loop controllers achieving the tracking of these 2 references by commanding these 3 inputs.

A. Closed-loop control of the IVT actuators

Ideally, the desired transmission ratio for each of the IVTs is obtained from a relationship similar to (3), yet generalized to our 2 degrees-of-freedom configuration: $\rho_{ref,t}(t) = \tau_{ref,l}(t)/\tau_{t,in}(t)$, assuming that $\tau_{t,in}$ can be properly measured. However, because the IVT is known to have non-ideal efficiency (see (6)), the actual torque transmitted to the

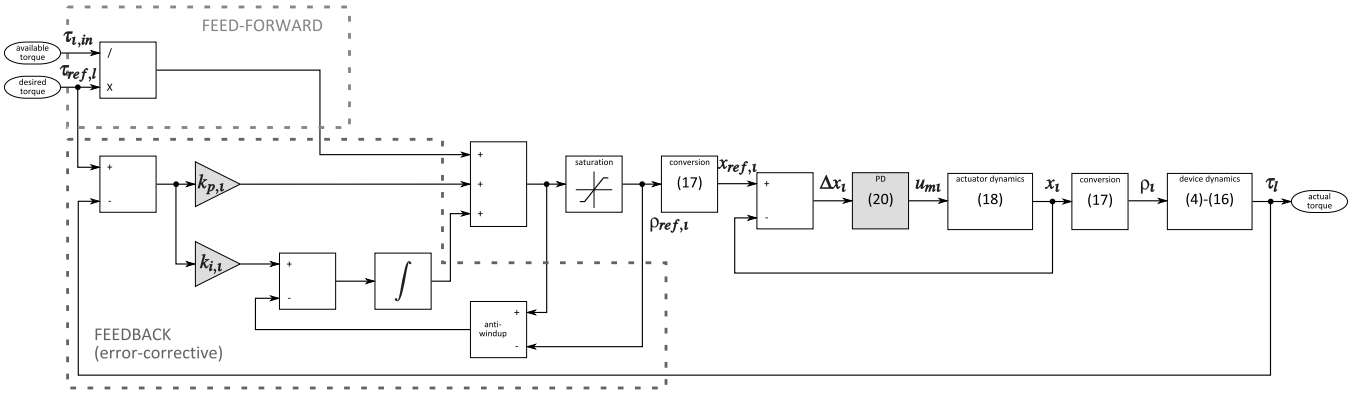

Fig. 3. Closed-loop controller of the IVT actuators. The shaded boxes highlight the controller gains. When appropriate, references to equations are provided in the blocs.

load τ_l will not be equal to $\tau_{ref,l}$. Therefore, the relationship between the reference output torque and the corresponding transmission ratio is augmented with error corrective terms:

$$\rho_{ref,\iota}(t) = \frac{\tau_{ref,l}(t)}{\tau_{\iota,in}(t)} + k_{p,\iota}(\tau_{ref,l}(t) - \tau_l(t)) + k_{i,\iota}\int(\tau_{ref,l}(t) - \tau_l(t))dt, \quad (19)$$

where $k_{p,\iota}$ and $k_{i,\iota}$ are, respectively, the proportional and integral gains of this error correction mechanism. There are little clues to achieve model-based synthesis of these gains, since the corresponding dynamics depends on the efficiency model and is thus highly non-linear. Next, $\rho_{ref,\iota}$ is saturated between the physical limits of the IVT, namely $\rho_{min,\iota}$ and $\rho_{max,\iota}$, and an anti-windup mechanism must be implemented to switch off the integral action when this saturation is reached.

Finally, this reference transmission ratio $\rho_{ref,\iota}$ is converted into a reference position of the IVT actuator $x_{ref,\iota}$ via (17). This reference position can be controlled via a classical proportional-derivative controller, whose transfer function is given by:

$$\frac{U_{m\iota}(s)}{\Delta X_\iota(s)} = k_{p,m\iota} + k_{d,m\iota}\frac{k_{n,m\iota}}{1+\frac{k_{n,m\iota}}{s}}, \quad (20)$$

where $\Delta X_\iota(s)$ is the Laplace transform of the position error, i.e. $\Delta x_\iota(t) = x_{ref,\iota}(t) - x_\iota(t)$, and $k_{p,m\iota}$, $k_{d,m\iota}$, and $k_{n,m\iota}$ are, respectively, the controller proportional and derivative gains, and the filter coefficient for the derivative action. Note that it is theoretically possible to achieve a model-based synthesis of these gains, since the corresponding open-loop dynamics are given by (18). In sum, an overview of the closed-loop controller of one IVT actuator is provided in Fig. 3.

B. Closed-loop control of the main power actuator

Since the IVT actuators already take care of transmitting the exact desired torques $\tau_{ref,l}$ to the joints, the purpose of the main power actuator controller is only to guarantee that the spring deformation never drops to 0 (see Section II). In order to achieve this, we implemented a closed-loop proportional-integral controller maintaining a desired deformation in the spring $\theta_{ref,s}$ (and thus a desired level of energy), i.e.:

$$u_m(t) = k_{p,m}(\theta_{ref,s} - \theta_s(t)) + k_{i,m}\int(\theta_{ref,s} - \theta_s(t))dt, \quad (21)$$

where $k_{p,m}$ and $k_{i,m}$ are, respectively, the proportional and integral gains of this controller. A similar anti-windup mechanism as the one pictured in Fig. 3 is moreover implemented to cope with voltage limits. Again, note that the closed-loop dynamics of this system can be – in theory – achieved through model-based gain synthesis, since the corresponding open-loop dynamics are given by (16). This requires however to treat both the friction torques and the load torque induced by the spring as unmodeled disturbances.

IV. RESULTS AND DISCUSSION

The numerical values that were given to the many parameters of this model are given in Table III. The rationales for selecting these values are reported in the following paragraphs.

The power motor parameters were taken from the datasheet of the 60W 'EC16-395558' brushless motor from Maxon Motor AG (Sachseln, Switzerland). Its gearbox parameters were taken from the datasheet of the 'GP22A-134162' from the same company. Note that we assumed the motor to have no friction ($\tau_f = 0$), so that energy losses in the power motor+gearbox are only captured by the gearbox non-ideal efficiency. Similarly, the IVT motors parameters were taken from the datasheet of the 30W 'EC16-400161' brushless motor from the same company.

The spring stiffness was selected to be quite compliant. If too stiff, large energy variations would correspond to large displacements on the motor side, thus not flattening the power profile. In contrast, a smaller stiffness would require to take a target spring deformation $\theta_{ref,s}$ that is not reachable with a physical spring, in order to store the appropriate amount of energy.

The geometrical parameters of the differential and IVTs were selected to be compliant with the IVT design of [17] and as a function of the torque peaks that have to be transmitted to the ankle and knee (see Fig. 1). The IVT

TABLE III

NUMERICAL VALUES GIVEN TO THE MODEL PARAMETERS. NUMBER IN PARENTHESES REFER TO THE CORRESPONDING EQUATIONS.

Power motor and gearbox: (16)	
equivalent inertia	$J_m = 1.47\,10^{-7}$ [kgm^2]
armature resistance	$R_m = 0.569$ [Ω]
back emf constant	$K_m = 5.25\,10^{-3}$ [Nm/A]
friction torque	$\tau_f = 0$ [Nm]
ratio	$\chi_g = 208.8$ [-]
efficiency	$\tilde{\eta_g} = 0.7$ [-]

Controller of the power motor: (21)	
P gain	$k_{p,m} = 1.29$ [V/rad]
I gain	$k_{i,m} = 0.395$ [V/(rad s)]

Compliant element (spring): (2)	
stiffness	$k = 0.04$ [Nm/rad]

Differential: (7-10)	
efficiency	$\tilde{\eta_d} = 0.95$ [-]
symmetry	$\chi_d = 0.546$ [-]

Ankle and knee IVTs: (6),(17),(18)	
efficiency	$\tilde{\eta_l} = 0.6$ [-]
planet angle	$\alpha = \pi/4$ [-]
lead screw pitch	$\xi = 1.43\,10^3$ [rad/m]

Ankle IVT only: (17),(19)	
min ratio	$\rho_{min,l1} = -1.5$ [-]
max ratio	$\rho_{max,l1} = 0.0335$ [-]
gear gain	$R_1 = 0.0145$ [m]

Knee IVT only: (17),(19)	
min ratio	$\rho_{min,l2} = -0.932$ [-]
max ratio	$\rho_{max,l2} = 0.253$ [-]
gear gain	$R_2 = 0.0112$ [m]

Motor of both IVTs: (18)	
equivalent inertia	$J_{ml} = 1.06\,10^{-7}$ [kgm^2]
armature resistance	$R_{ml} = 1.53$ [Ω]
back emf constant	$K_{ml} = 5.29\,10^{-3}$ [Nm/A]

Controller of both IVTs: (19-20)	
torque corrective term - P gain	$k_{p,l} = 0.4$ [1/Nm]
torque corrective term - I gain	$k_{i,l} = 0.016$ [1/(Nm s)]
actuator controller - P gain	$k_{p,ml} = 173$ [V/m]
actuator controller - D gain	$k_{d,ml} = -1.82$ [Vs/m]
actuator controller - D filter	$k_{n,ml} = 548$ [1/s]

efficiency was also taken from the experiments reported in [17] and other unpublished data.

The power motor controller gains were selected to achieve a closed-loop bandwidth of 0.6Hz with critical damping. This relatively small bandwidth (actually below the one of the tasks themselves, see Table I) was selected so that the spring could actually undergo large deformations, thus carrying out its duty of flattening the power profile.

In contrast, the power IVT controllers gains were selected to achieve a much higher closed-loop bandwidth, i.e. 60Hz, also with critical damping. In this case, the position closed-loop dynamics must be as high as possible, to make x_l following $x_{ref,l}$ with the lowest possible tracking error.

We simulated 20s of the closed-loop behavior of this transfemoral prosthesis in Matlab/Simulink (R2015a; the MathWorks, Natick, MA), for the three different tasks, and for a subject of 75kg. All simulations were generated by using the variable-step solver 'ode45'. The desired torque profiles $\tau_{ref,l}$ were constructed by concatenating several times the profiles of Fig. 1, and dividing this by a factor -100, capturing the effect of a final transmission stage (e.g. a lead screw) that was not accounted for in our model. Similarly, the resulting load velocities ω_l were constructed by concatenating the corresponding velocity profiles, this time multiplied by the same factor -100. Note that the laws governing the real-time efficiencies (Eqs. (6) and (10)) were actually replaced by smoother sigmoid functions, for numerical issues. These functions were such that they reach 95% of their plateaus for about $\pm$7W of transmitted output power. In the following, we report only graphs showing the steady-state regime, i.e. the last two of the simulated cycles.

For level-ground walking, the target spring deformation was set to $\theta_{ref,s} = 54.8$rad. This corresponds to an energy stored in the spring equal to $k\theta_{ref,s}^2/2 = 60$J, i.e. about twice the energy produced by the power motor during a level ground walking cycle. Fig. 4a reports the profiles of the power flows going through the different ports of the device. It highlights two important facts: (i) as power progresses

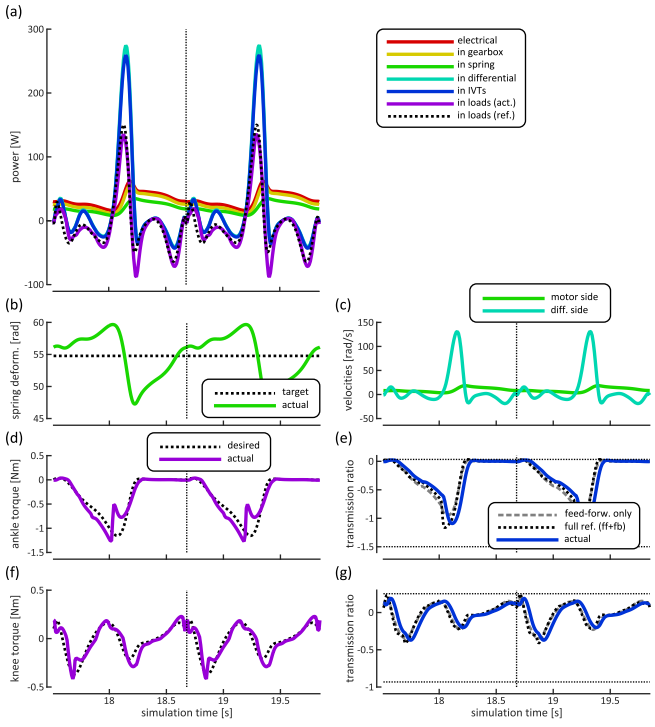

Fig. 4. Simulated level-ground walking. (a): profiles (as a function of time) of the power flows circulating between the different parts of the actuator, as represented in Fig. 2. (b): actual spring deformation $\theta_s(t)$, compared to the reference $\theta_{ref,s}$. (c): input ($\omega_m(t)$, motor side) and output ($\omega_{d,in}(t)$, differential side) shaft velocities, at both sides of the spring. (d): desired $\tau_{ref,l1}(t)$ and actual $\tau_{l1}(t)$ ankle torque. (e): transmission ratio of the ankle IVT: feed-forward only (i.e. the first term of (19)), full feedback-corrected reference $\rho_{ref,t1}(t)$ (i.e. all terms of (19)), and actual ratio $\rho_{t1}(t)$. (f,g): same as (d,e), for the knee joint. In (e,g), the horizontal lines represent the physical limits of the transmission ratios, i.e. $\rho_{min,t}$ and $\rho_{max,t}$. The vertical lines capture the separation between the two represented gait cycles.

TABLE IV

ENERGY BALANCE DURING THE LAST CYCLE OF THE POWER PROFILES REPORTED IN FIGS. 4A AND 5, IN JOULES. IF POSITIVE, ENERGY IS PRODUCED; IF NEGATIVE, IT IS DISSIPATED OR HARVESTED.

	Level-ground walking	Stair descending	Stair ascending
Electrical	38.9J	−50.4J	218.4J
in Gearbox	33.6J	−52.4J	173.8J
in Spring	23.8J	−74.9J	121.8J
in Differential	24.1J	−74.7J	121.6J
in Ankle IVT	28.7*J*	−7.8*J*	46.3*J*
in Knee IVT	−7.4*J*	−71.7*J*	68.7*J*
TOTAL	21.3J	−79.5J	115.1J
in Ankle load (ref)	11.1*J* (12.3*J*)	−27.1*J* (−24.5*J*)	25.4*J* (30.3*J*)
in Knee load (ref)	−19.9*J* (−16.7*J*)	−120.6*J* (−86.0*J*)	38.4*J* (50.3*J*)
TOTAL (ref)	−8.8J (−4.4J)	−147.7J (−110.4J)	63.7J (80.6J)

through the device (i.e. from the electrical power supplied to the actuator to the power actually measured across the loads), electrical and mechanical losses cause power drops; and (ii) the power profiles before the IVTs are much smoother than the ones after. Fact (i) is confirmed by Table IV, reporting the energy balance (i.e. the time-integral of the power curves) between the different parts. Note that the small discrepancy of energy balance at both sides of the spring (while the spring model was loss-less) is likely because the simulation did not reach a pure steady-state after 20 cycles. As expected, the largest power/energy drop is happening in the IVTs themselves, since their efficiency was equal to 60% only. Indeed, while the load energy balance is dissipative (19.9J are produced by the knee while only 11.1J are provided to the ankle), this balance is reversed at the other side of the IVTs: only 7.4J can be harvested from the knee IVT, while 28.7J must be supplied to the ankle IVT. At the end, the electrical actuator consumes 38.9J of electrical energy, so that the overall device efficiency is actually of −23%. This negative result should however be taken with care, since the current modeling of the IVT efficiency (see (6)) is only a crude image of the actual one. Indeed, a more realistic modeling of our IVT efficiency should make it dependent on the transmission ratio, so that higher efficiencies would be precisely faced when the largest amount of mechanical power has to be transmitted (see e.g. [21] for more details).

Fact (ii) is much more favorable for our design. Indeed the mechanical power supplied by the main actuator oscillates between 11.3W and 56.4W (with an electrical power supply varying from 16.2W to 62.0W), while the mechanical power transmitted to the loads fluctuates between −131.3W (knee) and 179W (ankle). The use of two IVTs, a differential, and a spring thus reduced the power peak by a factor 3. The spring plays a significant role in this mechanical buffering, storing an energy which varies between about 44.6J and 71.2J (see Fig. 4b). These fluctuations are caused by the large angular velocities of the spring output shaft, while the input shaft rotates with a much more stationary profile (see Fig. 4c), both being images of the corresponding power flows.

The torques being transmitted to both joints are reported in Fig. 4d,f. They are controlled via the IVTs transmission ratios ρ_{t1} and ρ_{t2}, reported in Fig. 4e,g. This highlights both the role of the feedback-driven terms of (19) correcting for the mechanical losses in the IVTs, and the closed-loop dynamics of the IVTs' actuators ((18) and (20)). Altogether, these dynamics explain the differences between the desired and actual joint torques (Fig. 4d,f), also giving rise to differences between the reference and actual power profiles (see Fig. 4a) and joint energy balance (see Table IV).

Fig. 4d,f reveals that the torques transmitted to the loads face significant drops at some phases of the cycle. This is particularly visible in the middle of the ankle negative torque peak. These drops happen when the load shaft velocity (and consequently, the power) crosses the zero line or, said differently, when there is a shift between energy production and dissipation and thus, according to (6), when the IVT efficiency abruptly switches to a different value. Again, it is likely that a real mechatronic device would behave differently: the torque drop would induce a drop in the shaft acceleration, and thus a smoother change in the load velocity and power. In sum, the loads model (see Section II-A) should be revisited to account for these complex dynamics.

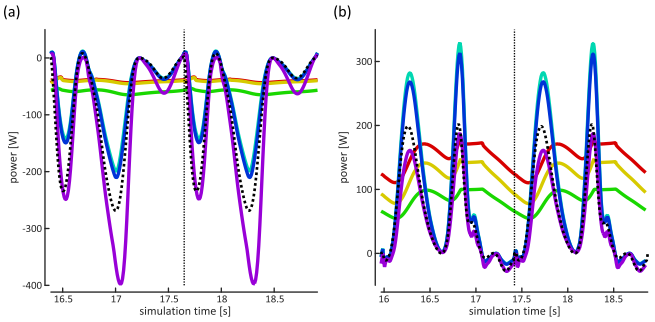

Fig. 5. Power profiles of simulated stair descent (a) and ascent (b). See Fig. 4a for the color code.

Fig. 5 shows the same power profiles as Fig. 4a, for both other tasks (stair descent/ascent). The corresponding energy balances are also reported in Table IV. The same observations as for level-ground walking can be reported: a dissipation of energy across the device, and a filtering of the power profile through the spring. Stair descent is purely dissipative: while 147.7J could be harvested from both joints during each of the cycles, only 50.4J can be harvested and potentially stored in the electrical battery. The device efficiency is thus equal to 34%. On the other hand, the power peak reduction is this time of about a factor 9.

Stair ascent requires – in contrast – to produce energy through both of the joints. More precisely, 63.7J are transmitted to the joints during a cycle, requiring to produce 218.4J of electrical energy. The global efficiency is thus, in this case, equal to 29%. This time, the power peak reduction is only of about a factor 1.3. Note that this last simulation required to

increase the target spring deformation to $\theta_{ref,s} = 141.4$rad, corresponding to a stored energy of 400J, i.e. again about twice larger than the energy spent by the electrical motor over a cycle. This increase was necessary in order to produce a larger spring torque, and thus to keep the transmission ratios within their respective boundaries. As a consequence, the motor current is higher, and thus the electrical losses within the motor are larger. Note finally that the peak power of the main actuator (180W as electrical and 148W as mechanical power) is much too high for the 60W motor that we selected in the simulated design. Improving this would require to improve the IVTs efficiency (again), to upgrade the device's main actuator, or to perform the stair ascending task at a slower pace than the one reported in Table I.

V. CONCLUSIONS

Motivated by the challenge to design light-weight and energy efficient lower-limb prostheses, this paper presented a novel actuation concept for a transfemoral prosthesis. It relied on two IVTs modulating the torque transmitted to both the ankle and knee joints, a mechanical differential conveying the energy flows in both directions (production/dissipation), and a single compliant element (spring) filtering the power profile between the load and the motor sides.

The paper reported a full modeling of this actuation principle, a preliminary approach for closed-loop control (tracking torque references at both joints), and simulation results of three representative locomotion tasks: level-ground walking, and stair ascending/descending. These tasks featured proper functionning of our prosthesis in different configurations: stair ascending (resp. descending) required to produce (resp. dissipate) energy at both joints, while level-ground walking was in-between. Although the simulated power profiles revealed a significant filtering across the spring, energy balances also revealed that the overall device efficiency requires to be improved.

Our current efforts are spent in the experimental validation of these results, both with a test bench, and with a prosthesis prototype. Whether such a device will be lighter or more efficient than another one with a standard actuation principle is still an open question. In parallel, we are working on the IVT concept reported in [17], in order to improve its efficiency.

ACKNOWLEDGMENT

We are grateful to the authors of [2] who accepted to share a digital version of the data reported in their paper.

REFERENCES

[1] C. Frigo, M. Rabuffetti, D. C. Kerrigan, L. C. Deming, and A. Pedotti, "Functionally oriented and clinically feasible quantitative gait analysis method." *Med Biol Eng Comput*, vol. 36, no. 2, pp. 179–185, Mar 1998.

[2] R. Riener, M. Rabuffetti, and C. Frigo, "Stair ascent and descent at different inclinations." *Gait Posture*, vol. 15, no. 1, pp. 32–44, Feb 2002.

[3] A. Matthys, P. Cherelle, M. Van Damme, B. Vanderborght, and D. Lefeber, "Concept and design of the hekta (harvest energy from the knee and transfer it to the ankle) transfemoral prosthesis," in *Biomedical Robotics and Biomechatronics (BioRob), 2012 4th IEEE RAS EMBS International Conference on*, june 2012, pp. 550 –555.

[4] R. Unal, F. Klijnstra, B. Burkink, S. Behrens, E. Hekman, S. Stramigioli, H. Koopman, and R. Carloni, "Modeling of walkmech: A fully-passive energy-efficient transfemoral prosthesis prototype," in *Rehabilitation Robotics (ICORR), 2013 IEEE International Conference on*, June 2013.

[5] B. J. Hafner, J. E. Sanders, J. M. Czerniecki, and J. Fergason, "Transtibial energy-storage-and-return prosthetic devices: a review of energy concepts and a proposed nomenclature." *J Rehabil Res Dev*, vol. 39, no. 1, pp. 1–11, 2002.

[6] S. H. Collins and A. D. Kuo, "Recycling energy to restore impaired ankle function during human walking." *PLoS One*, vol. 5, no. 2, p. e9307, 2010. [Online]. Available: http://dx.doi.org/10.1371/journal.pone.0009307

[7] D. A. Winter, *Biomechanics and motor control of human gait: normal, elderly and pathological*. University of Waterloo Press, 1991.

[8] R. Versluys, P. Beyl, M. V. Damme, A. Desomer, R. V. Ham, and D. Lefeber, "Prosthetic feet: state-of-the-art review and the importance of mimicking human ankle-foot biomechanics." *Disabil Rehabil Assist Technol*, vol. 4, no. 2, pp. 65–75, Mar 2009. [Online]. Available: http://dx.doi.org/10.1080/17483100802715092

[9] G. A. Pratt and M. M. Williamson, "Series elastic actuators," in *Proc. IEEE/RSJ International Conference on Intelligent Robots and Systems 95. 'Human Robot Interaction and Cooperative Robots'*, vol. 1. Institute of Electrical and Electronics Engineers (IEEE), Aug. 5–9, 1995, pp. 399–406. [Online]. Available: http://dx.doi.org/10.1109/IROS.1995.525827

[10] M. Eilenberg, H. Geyer, and H. Herr, "Control of a powered ankle-foot prosthesis based on a neuromuscular model," *IEEE Trans Neural Syst Rehabil Eng*, vol. 18, no. 2, pp. 164–173, april 2010.

[11] H. M. Herr and A. M. Grabowski, "Bionic ankle-foot prosthesis normalizes walking gait for persons with leg amputation." *Proc Biol Sci*, vol. 279, no. 1728, pp. 457–464, Feb 2012. [Online]. Available: http://dx.doi.org/10.1098/rspb.2011.1194

[12] F. Sup, H. A. Varol, and M. Goldfarb, "Upslope walking with a powered knee and ankle prosthesis: initial results with an amputee subject." *IEEE Trans Neural Syst Rehabil Eng*, vol. 19, no. 1, pp. 71–78, Feb 2011. [Online]. Available: http://dx.doi.org/10.1109/TNSRE.2010.2087360

[13] J. Geeroms, L. Flynn, R. Jimenez-Fabian, B. Vanderborght, and D. Lefeber, "Ankle-knee prosthesis with powered ankle and energy transfer for cyberlegs alpha-prototype," in *Rehabilitation Robotics (ICORR), 2013 IEEE International Conference on*. Institute of Electrical and Electronics Engineers (IEEE), June 2013.

[14] S. Stramigioli, G. van Oort, and E. Dertien, "A concept for a new energy efficient actuator," in *Proc. IEEE/ASME Int. Conf. Advanced Intelligent Mechatronics AIM 2008*, 2008, pp. 671–675.

[15] C. Everarts, B. Dehez, and R. Ronsse, "Variable stiffness actuator applied to an active ankle prosthesis: Principle, energy-efficiency, and control," in *Intelligent Robots and Systems (IROS), 2012 IEEE/RSJ International Conference on*, oct. 2012, pp. 323–328.

[16] L. Mooney and H. Herr, "Continuously-variable series-elastic actuator," in *Proc. IEEE 13th Int. Conf. Rehabilitation Robotics (ICORR)*, June 2013.

[17] C. Everarts, B. Dehez, and R. Ronsse, "Novel infinitely variable transmission allowing efficient transmission ratio variations at rest," in *Intelligent Robots and Systems (IROS), 2015 IEEE/RSJ International Conference on*, Sept 2015, pp. 5844–5849.

[18] O. Gerelli, R. Carloni, and S. Stramigioli, "Port-based modeling and optimal control for a new very versatile energy efficient actuator," in *Proceedings of the Symposium on Robot Control*, vol. 42, no. 16. Japan: Elsevier BV, September 2009, pp. 493–498. [Online]. Available: http://dx.doi.org/10.3182/20090909-4-jp-2010.00084

[19] C. Pelchen, C. Schweiger, and M. Otter, "Modeling and simulating the efficiency of gearboxes and of planetary gearboxes," in *Modelica 2002*. Oberpfaffenhofen, Germany: The Modelica Association, March 18-19 2002, pp. 257–266.

[20] M. W. Spong, S. Hutchinson, and M. Vidyasagar, *Robot Modeling and Control*. Wiley, 2006. [Online]. Available: http://www-cvr.ai.uiuc.edu/ seth/SHV/

[21] G. Mantriota, "Performances of a series infinitely variable transmission with type i power flow," *Mechanism and Machine Theory*, vol. 37, no. 6, pp. 579 – 597, 2002. [Online]. Available: http://www.sciencedirect.com/science/article/pii/S0094114X02000174